Suppression of transport anisotropy at the Anderson localization transition in three-dimensional anisotropic media

Antton Goïcoechea [1], Sergey E. Skipetrov [2], and John H. Page [1,*]

[1]*Department of Physics and Astronomy, University of Manitoba, Winnipeg, Manitoba, Canada R3T 2N2*
[2]*Université Grenoble Alpes, CNRS, LPMMC, 38000 Grenoble, France*

We study the transport of classical waves through three-dimensional (3D) anisotropic media close to the Anderson localization transition. Time-, frequency-, and position-resolved ultrasonic measurements are performed on anisotropic slab-shaped mesoglass samples to probe the dynamics and the anisotropy of the multiple scattering halo, and hence to investigate the influence of disorder on the nature of wave transport and its anisotropy. These experiments allow us to address conflicting theoretical predictions that have been made about whether or not the transport anisotropy is affected by the interference effects that lead to Anderson localization. We find that the transport anisotropy is significantly reduced as the mobility edge is approached—a behavior similar to the one predicted recently for matter waves in infinite anisotropic 3D media.

The transport of a wave—quantum or classical—through a disordered medium can be inhibited by interference effects, a phenomenon known as Anderson localization [1–3]. In three-dimensional (3D) systems, and only in 3D for the orthogonal symmetry class for which no particular symmetry is broken, a transition occurs between the extended regime (diffusive transport) and the localization regime (exponentially suppressed transport) when the disorder is increased [4]. For classical waves, the localization regime is difficult to reach due to the very strong scattering needed to observe it; typically the scattering strength $k\ell_s$ has to be close to 1 (where k is the wave number and ℓ_s is the scattering mean free path) according to the Ioffe-Regel criterion [5,6]. Anderson localization might be easier to achieve in strongly anisotropic media because of the reduced effective dimensionality [7,8]. In such media, the scaling behavior is expected to be the same as in isotropic systems, and a single critical point remains. The effect of the anisotropy on the transition is nevertheless not trivial and there has been a lot of effort to incorporate it in numerical models, in particular in the context of cold atoms [9]. Additionally, early theoretical work using the self-consistent (SC) theory of localization predicted that the transport anisotropy (defined as the ratio of the diffusion tensor's components) is not affected by interference effects [10,11]. This view has been challenged in Ref. [12], in which the authors use a more sophisticated version of the SC theory (see also Ref. [13]) and predict that the transport anisotropy is significantly reduced if not vanishingly small at the mobility edge. The question concerning the influence of the anisotropy on the transport of waves in very strongly scattering disordered systems is therefore not settled, motivating us to investigate it experimentally using ultrasound.

Ultrasonic waves have proven to be advantageous to observe localization [14–19], whereas 3D localization of light remains elusive [20,21]. Because we work with excitations of energy much exceeding both the single phonon energy hf and the thermal energy k_BT at room temperature T, our experiments can be interpreted using a classical wave equation and do not require low T to be meaningful. This is an important advantage with respect to quantum waves (electrons or cold atoms) and allows us to relax all the constraints inherent to low-temperature experiments. We also do not have to worry about interactions, present for electrons and cold atoms and having drastic effects on the transport properties (many-body localization, for example), provided that we stay in the linear regime of wave propagation. The length scales involved are also arguably more convenient since for typical ultrasonic experiments the wavelength is of the order of a millimeter for the wave frequency $f \sim 1$ MHz. The characteristic lengths in the samples are therefore between a fraction of a millimeter and a few centimeters, whereas the length scales in optical or matter wave experiments are orders of magnitude shorter. The amplitude and phase of acoustic signals can also be measured directly, which is generally very difficult in optics (in most experiments only the intensity is measured). Finally, time-, frequency-, and position-resolved ultrasonic experiments have been designed to measure transport quantities without the measurements being hindered by absorption [19,22]. Using these techniques, we study experimentally, close to the Anderson localization transition, two anisotropic samples with differently oriented structural anisotropy, and focus in particular on the evolution of the transport anisotropy upon approaching the mobility edge. Our experiments provide a clear answer to the question of whether or not the transport anisotropy is significantly modified as the Anderson transition is approached.

Our slab-shaped samples are made of elongated, roughly ellipsoidal, aluminum particles brazed together. The method

---

to fabricate the samples is covered in detail in Refs. [23–25]. The links between the particles strongly influence the scattering strength of the resulting network. Once a sample is fabricated, it is possible to enhance sound scattering in it by etching the links by putting the sample in hydrochloric acid. Etching makes it possible to reach the critical regime near the Anderson localization transition. By comparing the highly reflective surface area of the polished outside surfaces with the highly reflective surface area of the inside cut surfaces of test samples, using the image-analysis software IMAGEJ [26] to measure the fraction of the total image area due to aluminum, we verified that the etching process is uniform.

The first sample investigated (A1) is made of small aluminum particles (approximately $3 \text{ mm} \times 1.5 \text{ mm} \times 1.5 \text{ mm}$) aligned along the z axis that is perpendicular to the slab. After etching, the density of this sample is 1.269 g/cm^3 (the aluminum volume fraction is approximately 47%). The second sample (A2) consists of bigger aluminum particles (approximately $4 \text{ mm} \times 2 \text{ mm} \times 2 \text{ mm}$) with the long axis of the particles aligned along the y axis in the plane of the slab. The density of this sample after etching is 1.002 g/cm^3 (the aluminum volume fraction is approximately 37%). The scattering strength $k\ell_s$ in strongly scattering acoustic samples can be estimated from measurements of the average transmitted wave field [27,28]. In our anisotropic samples, the scattering is so strong that the challenge of separating the average field from the multiply scattered waves makes the estimation difficult. Nonetheless, the data suggest that $k\ell_s \sim 1$ for A1e (where "e" stands for "etched"), and $k\ell_s \sim 2$ for A2e at the frequencies of interest. These values indicate very strong scattering and are close to the Ioffe-Regel criterion of localization $k\ell_s \sim 1$ [5,6].

To study the transport of ultrasound in our anisotropic samples, we measure the time dependence of the transmitted intensity profile for a pointlike excitation at the origin $x = y = z = 0$. This quantity has been measured previously in isotropic samples made of aluminum beads to investigate Anderson localization of ultrasonic waves without being obscured by absorption [14,19]. Experimentally, the transmitted acoustic field $\psi(\boldsymbol{\rho}, t)$ is measured at nine detector positions near the sample surface $z = L$: $\boldsymbol{\rho} = (x, y) = \{(0, 0), (\pm 15, 0), (\pm 20, 0), (0, \pm 15), (0, \pm 20)\}$ mm, for $55 \times 55 = 3025$ different source positions at the opposite slab surface $z = 0$. For each measurement, the origin of the reference frame is fixed at the source position. The separation between the source positions on the grid is equal to about one wavelength, enabling averaging over source positions to be done to estimate ensemble averages. The average transmitted intensity $I(\boldsymbol{\rho}, t) \propto \langle |\psi(\boldsymbol{\rho}, t)|^2 \rangle$ is then used to calculate the transverse width squared:

$$w_{\boldsymbol{\rho}}^2(t) = -\rho^2 / \ln \left[\frac{I(\boldsymbol{\rho}, t)}{I(0, t)} \right], \quad (1)$$

where t denotes propagation time through the sample and $\rho = \sqrt{x^2 + y^2}$. In the diffusive regime and for isotropic transport, $I(\boldsymbol{\rho}, t) = I(\rho, t)$ and the width squared is simply $w_{\boldsymbol{\rho}}^2(t) = 4Dt$, where D is the diffusion coefficient of ultrasound. In the localization regime, the wave is confined in the transverse direction and the width squared saturates at long times [29]. The width squared is therefore a direct measure of the dynamic

spread of the wave through the sample and of its confinement by localization effects, if present.

We are mainly interested in the variation of the transport anisotropy as the mobility edge is approached. In the diffusive regime, the anisotropy can be quantified by the ratio of the different elements D_{xx}, D_{yy}, and D_{zz} of the (diagonal) diffusion tensor D, irrespective of whether the medium is finite or not. As one gets closer to the localization transition, this way of quantifying transport anisotropy becomes ill-adapted to experimental studies, since the ratio of the elements of D is not directly accessible and may not even be uniquely defined in finite-sized samples, where D becomes position dependent. Moreover, for sample A1, the transport anisotropy is not directly visible in the intensity profile $I(\boldsymbol{\rho}, t)$ and requires a careful comparison with theoretical models to be assessed. In contrast, for sample A2, the anisotropy is in the plane of the slab and is thus expected to manifest itself by a deviation of $I(\boldsymbol{\rho}, t)$ from a circularly symmetric shape, leading to a difference between $w_x^2(t)$ and $w_y^2(t)$, which are shorthand notations for $w_{\boldsymbol{\rho}}^2$ with $\boldsymbol{\rho} = (x, 0)$ and $\boldsymbol{\rho} = (0, y)$, respectively. We can therefore define a parameter $\mathcal{A}_\rho$ characterizing the transport anisotropy as

$$\mathcal{A}_\rho = \lim_{t \to \infty} \frac{w_y^2(t)}{w_x^2(t)} \bigg|_{x = y = \rho}. \quad (2)$$

In the diffusive regime this is equivalent to $\mathcal{A}_\rho = D_{yy}/D_{xx}$.

We first present the results for sample A1, for which the long axis of the particles is parallel to the z axis and $D_{xx} = D_{yy} = D_\perp \neq D_{zz}$. Before etching, the transport near $f = 1$ MHz is diffusive ($w_{\boldsymbol{\rho}}^2 \propto t$), with significant anisotropy. Fits of the experimental data for $I(\rho, t)$ and $w_{\boldsymbol{\rho}}^2(t)$ with the diffusion theory yield the transport anisotropy $D_{zz}/D_\perp \simeq 2.5$. In contrast, after etching, a completely different behavior is found, with $w_{\boldsymbol{\rho}}^2(t)$ bending over significantly with time at all investigated frequencies f from 0.4 to 1.3 MHz. Representative data at 0.5 and 1.2 MHz are shown in Fig. 1, where at both frequencies $w_{\boldsymbol{\rho}}^2(t)$ tends to saturate with time at a low value $w_{\boldsymbol{\rho}}^2(t \to \infty)/L^2 \leqslant 1$. Note that SC theory predicts $w_{\boldsymbol{\rho}}^2(t \to \infty)/L^2 \sim 1$ for thick isotropic samples at the mobility edge [29]. Thus, Fig. 1 clearly indicates that the transport is not diffusive for sample A1e, and that localization is close to taking place in this frequency range, with the tendency of the width squared to saturate being more pronounced at 1.2 MHz. At both frequencies, $w_{\boldsymbol{\rho}}^2(t)$ depends on the value of ρ, which is the expected behavior near a mobility edge [14].

The absence of a transport theory for anisotropic media of finite size makes it challenging to determine with certainty whether Anderson localization has been reached in sample A1e. Nevertheless, the significant deviations from classical diffusion observed in Fig. 1 are likely to be accompanied by a suppression of transport anisotropy according to the recent theoretical work [12]. It is then tempting to fit the data with the SC theory for isotropic media. Indeed, if the anisotropy does disappear, then we could expect the theory to work. Note that for isotropic systems, comparison of this theory with experimental data for $I(\rho, t)$ and $w_{\boldsymbol{\rho}}^2(t)$ has enabled the localized and extended regimes to be distinguished, and mobility edges identified [14,18,19]. Proximity to a mobility edge is conveniently assessed by the localization length ξ
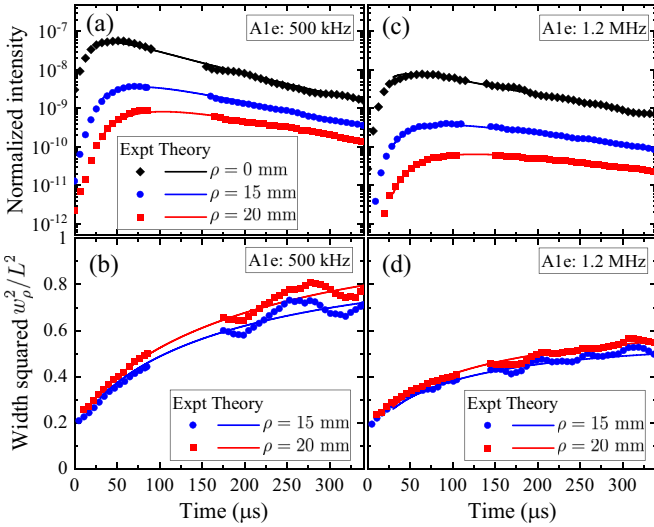
FIG. 1. (a), (c) Time of flight (TOF) profiles $I(\rho, t)$ and (b), (d) width squared $w_\rho^2(t)$ as functions of time for the etched sample A1e at 0.5 and 1.2 MHz, respectively (bandwidth of 50 kHz). Symbols represent experimental data and solid lines represent fits with the isotropic SC theory. The legend for (a) also applies to (c). The missing data near 125 μs are not shown because of contamination by a spurious electronic pickup pulse. At 0.5 MHz, the best fits are obtained for $L/\zeta = 0.5$ [$k\ell_s > (k\ell_s)_c$]; at 1.2 MHz, we obtain $L/\xi = 2.5$ [$k\ell_s < (k\ell_s)_c$]. The good quality of fits suggests that the transport is diffusive (although strongly renormalized by localization effects) at 0.5 MHz and that Anderson localization is reached at 1.2 MHz. The good fit quality also suggests that the transport anisotropy is greatly reduced at both frequencies.

when $k\ell_s < (k\ell_s)_c$ (localization regime) and the correlation length of fluctuations ζ when $k\ell_s > (k\ell_s)_c$ (diffusive regime) [19]. Here $(k\ell_s)_c \sim 1$ is the value of $k\ell_s$ at the mobility edge [30]. Both ξ and ζ diverge at the mobility edge.

Fits of excellent quality are obtained when the isotropic SC theory is used to fit the experimental data for sample A1e (see Fig. 1). At 0.5 MHz [Figs. 1(a) and 1(b)], the best fits are found for $L/\zeta = 0.5$ [$k\ell_s/(k\ell_s)_c = 1.003$], consistent with the system being still in the extended regime but very close to the mobility edge at this frequency. We can also infer, since the fits are good, that the transport anisotropy is greatly reduced this close to the mobility edge (recall that $D_{zz}/D_\perp \simeq 2.5$ for this sample before etching). At 1.2 MHz [Figs. 1(c) and 1(d)] the best fits are found for $L/\xi = 2.5$ [$k\ell_s/(k\ell_s)_c = 0.988$], indicating Anderson localization of ultrasound. Thus, not only do the good fits obtained using the isotropic SC theory with $L/\xi = 2.5$ indicate that Anderson localization has been achieved, but they also show that the transport anisotropy must be so greatly reduced in the localization regime that it has negligible impact on the fit quality.

To obtain information on the evolution of the transport anisotropy in the approach to localization in a more direct way, we now turn to sample A2, for which the anisotropy is in the plane of the slab (particles' major axis parallel to the y axis). The behavior of the width squared, as a function of structural disorder and frequency, is illustrated in Fig. 2, which shows a comparison of the widths squared for both the unetched and etched samples, at four different frequencies
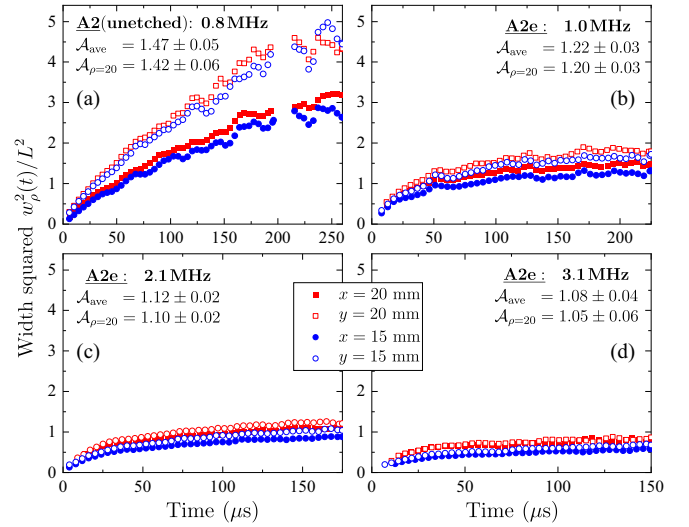

FIG. 2. Comparison of width squared for samples A2 and A2e at several frequencies, up to the maximum frequency at which the transmitted signals were large enough for $w_\rho^2(t)$ to be measured. As the frequency increases, the widths squared bend over more and more, and the difference between $w_x^2(t)$ and $w_y^2(t)$ decreases, giving a clear visualization of the reduction in transport anisotropy as the Anderson transition is approached.

and for two ρ values. For the unetched sample A2 [panel (a)], the width squared at 800 kHz shows only modest deviations from the linear growth in time that is characteristic of purely diffuse behavior, and the separation between the width squared for $\boldsymbol{\rho} = (x = \rho, 0)$ and $\boldsymbol{\rho} = (0, y = \rho)$ is large (compare closed and open symbols of the same color and type). For the etched sample A2e, the transverse spreading of wave energy is much slower, with $w_\rho^2(t)$ bending over significantly as time increases, at all frequencies. In particular, as the frequency is increased, $w_x^2(t)$ and $w_y^2(t)$ bend over more and more, and get closer and closer together. Notably, at 3.1 MHz, the width squared indicates substantial confinement of the wave energy and the values corresponding to the two different directions are very close to each other, showing that the transport anisotropy has almost vanished. These observations demonstrate that the etching has increased the disorder inside the sample, and that it is reasonable to expect that the mobility edge is close to 3.1 MHz (because the width squared looks like it is about to saturate at long times). Thus, as the width squared approaches the behavior expected at the mobility edge (saturation at a constant value $\sim L^2$ as $t \to \infty$), the anisotropy is progressively reduced and appears to have almost disappeared at 3.1 MHz.

The anisotropy $\mathcal{A}_\rho$ is shown in Fig. 3 as a function of frequency for both the unetched and etched samples. The evolution of the anisotropy is indicated by symbols for two transverse distances $\rho = 15$ and 20 mm, while the dotted curve denotes their average. This direct measurement clearly demonstrates that there is a substantial decrease of the anisotropy as the frequency, and hence the effective disorder strength, is increased. In particular, it is interesting to look at the differences in the measured anisotropy with transverse distance. At $\rho = 20$ mm, the anisotropy continues to decrease
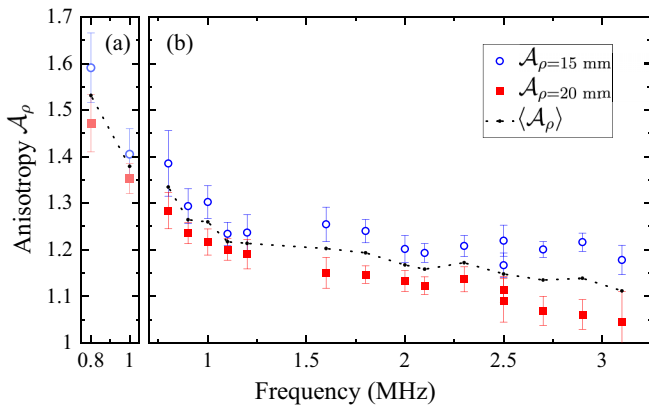
FIG. 3. Comparison of the transport anisotropy defined by Eq. (2) as a function of frequency for samples A2 in panel (a) and A2e in panel (b). The anisotropy measured separately for $\rho = 20$ mm and $\rho = 15$ mm is presented with symbols while the average anisotropy for transverse distances of 15 and 20 mm is shown by the dotted lines. As the frequency increases, leading to an increase in the effective disorder (see the effect on the width squared in Fig. 2), the anisotropy decreases, with $\mathcal{A}_\rho$ approaching 1 (no anisotropy) at the highest frequency for which data could be obtained. The decrease in anisotropy is more pronounced at the greater transverse distance of $\rho = 20$ mm.

as the highest attainable frequency of 3.1 MHz is reached and appears to extrapolate to 1 at a slightly higher frequency. (At 3.1 MHz, $\mathcal{A}_{\rho=20} = 1.045 \pm 0.065$, and is actually consistent with 1 even at this frequency.) However, at $\rho = 15$ mm, the anisotropy is larger at all frequencies, and its decrease in the upper part of the accessible frequency range is less obvious. These data strongly suggest that as the localization transition is approached, the shape of the multiply scattering halo $I(\boldsymbol{\rho}, t)$ changes: it remains somewhat anisotropic near $\boldsymbol{\rho} = 0$ but its anisotropy appears to nearly vanish at large distances ρ. It is tempting to consider that large distances ρ may capture more closely in a finite sample the situation encountered in the infinite medium, where the SC theory has predicted that the transport anisotropy is strongly suppressed or even vanishes at

the mobility edge [12]. Thus, our experiments seem to confirm the predictions of Piraud *et al.* [12]. In addition, our results demonstrate that in real samples, which are necessarily of finite size, the way in which the suppression of the anisotropy shows up is more complex.

In summary, we have shown that samples made of elongated aluminum particles, aligned along a given direction, are suitable to investigate Anderson localization of ultrasound in anisotropic media. To assess the transport anisotropy, we have proposed a generalized definition in terms of the anisotropy in the width of the multiple scattering halo, which reduces to the standard definition as a diffusion coefficient ratio in diffuse media but has the advantage of being directly measurable experimentally for finite samples in both the extended and localization regimes. Thus, we have demonstrated that the transport anisotropy is significantly reduced as the mobility edge is approached and that the wave transport tends towards isotropic behavior very close to the localization transition. This work constitutes a clear experimental observation of this behavior, and supports the recent SC theory predictions for infinite media [12]. Our findings indicate that the "ellipsoidal" cutoff in the SC theory used in Refs. [10,11] may not be valid, as the predictions it produces are not consistent with our data. It is worth mentioning that our anisotropic samples feature a much more gradual approach to the localization regime as the frequency is varied than what was observed in previously studied samples made of aluminum beads [19]. This is likely due to the irregular shape and the polydispersity of the anisotropic particles, as well as to the control over the scattering strength (via the brazing conditions and postfabrication etching of the samples) that enabled the critical regime to be reached. This result motivates further experimental work with such samples to explore their behavior near the mobility edge; assuming such experiments are successful and sufficient configurational averaging can be achieved, a finite-time scaling analysis could be performed in order to extract the critical exponent of the Anderson transition [31,32].

[1] P. W. Anderson, Absence of diffusion in certain random lattices, Phys. Rev. **109**, 1492 (1958).

[2] *50 years of Anderson localization*, edited by E. Abrahams (World Scientific, Singapore, 2010).

[3] P. Sheng, *Introduction to Wave Scattering, Localization and Mesoscopic Phenomena* (Springer Science & Business Media, Berlin, 2006), Vol. 88.

[4] E. Abrahams, P. W. Anderson, D. C. Licciardello, and T. V. Ramakrishnan, Scaling Theory of Localization: Absence of Quantum Diffusion in Two Dimensions, Phys. Rev. Lett. **42**, 673 (1979).

[5] A. F. Ioffe and A. R. Regel, in *Progress in Semiconductors*, edited by A. F. Gibson (Wiley, New York, 1960), Vol. 4, pp. 237–291.

[6] S. E. Skipetrov and I. M. Sokolov, Ioffe-Regel criterion for Anderson localization in the model of resonant point scatterers, Phys. Rev. B **98**, 064207 (2018).

[7] A. A. Abrikosov, Anderson localization in strongly anisotropic metals, Phys. Rev. B **50**, 1415 (1994).

[8] B. C. Kaas, B. A. van Tiggelen, and A. Lagendijk, Anisotropy and Interference in Wave Transport: An Analytic Theory, Phys. Rev. Lett. **100**, 123902 (2008).

[9] M. Pasek, G. Orso, and D. Delande, Anderson Localization of Ultracold Atoms: Where is the Mobility Edge? Phys. Rev. Lett. **118**, 170403 (2017).

[10] P. Wölfle and R. N. Bhatt, Electron localization in anisotropic systems, Phys. Rev. B **30**, 3542 (1984).

[11] R. N. Bhatt, P. Wölfle, and T. V. Ramakrishnan, Localization and interaction effects in anisotropic disordered electronic systems, Phys. Rev. B **32**, 569 (1985).

[12] M. Piraud, L. Sanchez-Palencia, and B. A. van Tiggelen, Anderson localization of matter waves in three-dimensional anisotropic disordered potentials, Phys. Rev. A **90**, 063639 (2014).

[13] A. Yedjour and B. A. van Tiggelen, Diffusion and localization of cold atoms in 3D optical speckle, Eur. Phys. J. D **59**, 249 (2010).

[14] H. Hu, A. Strybulevych, J. H. Page, S. E. Skipetrov, and B. A. van Tiggelen, Localization of ultrasound in a three-dimensional elastic network, Nat. Phys. **4**, 945 (2008).

[15] S. Faez, A. Strybulevych, J. H. Page, A. Lagendijk, and B. A. van Tiggelen, Observation of Multifractality in Anderson Localization of Ultrasound, Phys. Rev. Lett. **103**, 155703 (2009).

[16] W. K. Hildebrand, A. Strybulevych, S. E. Skipetrov, B. A. van Tiggelen, and J. H. Page, Observation of Infinite-Range Intensity Correlations above, at, and below the Mobility Edges of the 3D Anderson Localization Transition, Phys. Rev. Lett. **112**, 073902 (2014).

[17] A. Aubry, L. A. Cobus, S. E. Skipetrov, B. A. van Tiggelen, A. Derode, and J. H. Page, Recurrent Scattering and Memory Effect at the Anderson Localization Transition, Phys. Rev. Lett. **112**, 043903 (2014).

[18] L. A. Cobus, S. E. Skipetrov, A. Aubry, B. A. van Tiggelen, A. Derode, and J. H. Page, Anderson Mobility Gap Probed by Dynamic Coherent Backscattering, Phys. Rev. Lett. **116**, 193901 (2016).

[19] L. A. Cobus, W. K. Hildebrand, S. E. Skipetrov, B. A. van Tiggelen, and J. H. Page, Transverse confinement of ultrasound through the Anderson transition in three-dimensional mesoglasses, Phys. Rev. B **98**, 214201 (2018).

[20] S. E. Skipetrov and I. M. Sokolov, Absence of Anderson Localization of Light in a Random Ensemble of Point Scatterers, Phys. Rev. Lett. **112**, 023905 (2014).

[21] S. E. Skipetrov and J. H. Page, Red light for Anderson localization, New J. Phys. **18**, 021001 (2016).

[22] J. H. Page, H. P. Schriemer, A. E. Bailey, and D. A. Weitz, Experimental test of the diffusion approximation for multiply scattered sound, Phys. Rev. E **52**, 3106 (1995).

[23] H. Hu, Localization of ultrasonic waves in an open three-dimensional system, Master's thesis, University of Manitoba, 2006.

[24] L. A. Cobus, Anderson localization and anomalous transport of ultrasound in disordered media, Ph.D. thesis, University of Manitoba, 2016.

[25] S. Kerherve, Transport of ultrasonic waves in strongly scattering or absorbing heterogeneous media, Ph.D. thesis, University of Manitoba, 2018.

[26] ImageJ. An open platform for scientific image analysis, https://imagej.net/ (2018), accessed November 4, 2020.

[27] J. H. Page, P. Sheng, H. P. Schriemer, I. Jones, X. Jing, and D. A. Weitz, Group velocity in strongly scattering media, Science **271**, 634 (1996).

[28] M. L. Cowan, K. Beaty, J. H. Page, Z. Liu, and P. Sheng, Group velocity of acoustic waves in strongly scattering media: Dependence on the volume fraction of scatterers, Phys. Rev. E **58**, 6626 (1998).

[29] N. Cherroret, S. E. Skipetrov, and B. A. van Tiggelen, Transverse confinement of waves in three-dimensional random media, Phys. Rev. E **82**, 056603 (2010).

[30] See, for example, Ref. [19] for the relationships between ξ, ζ, $k\ell_s$, and $(k\ell_s)_c$.

[31] G. Lemarié, J. Chabé, P. Szriftgiser, J. C. Garreau, B. Grémaud, and D. Delande, Observation of the Anderson metal-insulator transition with atomic matter waves: Theory and experiment, Phys. Rev. A **80**, 043626 (2009).

[32] Y. M. Beltukov and S. E. Skipetrov, Finite-time scaling at the Anderson transition for vibrations in solids, Phys. Rev. B **96**, 174209 (2017).